GSA Data Repository 2017326

Publisher: GSA
Journal: Geology
DOI:10.1130/G39367.1

Supplemental Information for "Preserving proxy records in dynamic landscapes: Modeling and examples from the Paleocene-Eocene Thermal Maximum"

Sheila M. Trampush[1*] and Elizabeth A. Hajek[1]

[1]*Department of Geosciences, Pennsylvania State University, University Park, Pennsylvania 16802, USA*

[*] Corresponding author: smt254@psu.edu

Contents

1. Introduction

This document is a selection of tables and figures that support the main conclusions and discussion points in our article "Climate signals from proxy records are influenced by variability in sedimentation". We also provide links for the data and model we created and used in the manuscript. Material is arranged topically in the order presented in the manuscript.

2. PETM Bulk Organic Records

We compiled 15 bulk organic carbon isotope curves from the Bighorn basin in Wyoming, the Piceance basin in Colorado, the Californian margin, the Tremp-Gaus and Basque-Cantabrian basins from northern Spain, and from the Southern Ocean (John et al., 2008; Sluijs et al., 2011; Foreman et al., 2012; Baczynski et al., 2013; Manners et al., 2013). A text file of the compilation is available at https://scholarsphere.psu.edu/files/wm117p117.

3. Sedimentation Rates and Variability from Modern Systems

We calibrated the input parameters for our stochastic sedimentation model using observations from extant and ancient systems. Sedimentation rates from a variety of tectonic settings inform our "high sedimentation" and "low sedimentation" scenarios (Table S1). We used measurements and models of event deposition in shelf and fluvial environments to scale the "high-sedimentation-variability" and "low-sedimentation-variability" model scenarios (Table S2).

Table S1: Sedimentation rates from modern and ancient depositional systems

Environment	Location	Sedimentation rate (mm/yr)	How sedimentation rate was measured	Citation
Shelf	Monterey shelf, U.S.A.	1-4	^{210}Pb	(Lewis et al., 2002)
Pro-delta	Brazos River pro-delta, U.S.A.	1-5	^{210}Pb	(Carlin and Dellapenna, 2014)
Shelf	Eel River shelf, U.S.A.	2-14 mean= 4	^{210}Pb	(Sommerfield and Nittrouer, 1999)
Shelf	Waipaoa River margin, New Zealand	2-20	^{210}Pb	(Rose and Kuehl, 2010; Hale et al., 2014; Walsh et al., 2014)
Shelf	Palos Verde Shelf, U.S.A.	5	Sediment transport model	(Ferré et al., 2010)
Shelf	Eocene Marlboro Clay, North Atlantic Margin, Maryland, U.S.A.	0.1- 0.3	Biostratigraphy	(Kopp et al., 2009; Self-Trail et al., 2012)
Shelf	Eocene Marlboro Clay, North Atlantic Margin, New Jersey, U.S.A.	0.1	Biostratigraphy	(Sluijs and Brinkhuis, 2009)
Deltaic	Rio Grande River delta	0.71	NA	Cited in: (Straub and Wang, 2013)
Deltaic	Niger River delta	0.71	NA	Cited in: (Straub and Wang, 2013)
Deltaic	Orinoco River delta	2.7	NA	Cited in: (Straub and Wang, 2013)
Deltaic	Po River delta	1.0	NA	Cited in: (Straub and Wang, 2013)
Deltaic	Rhine River delta	0.15	NA	Cited in: (Straub and Wang, 2013)
Deltaic	Baram River delta	0.43	NA	Cited in: (Straub and Wang, 2013)
Deltaic	Nile River delta	0.39	NA	Cited in: (Straub and Wang, 2013)
Deltaic	Yellow River delta	0.6	NA	Cited in: (Straub and Wang, 2013)
Deltaic	Mackenzie River delta	0.12	NA	Cited in: (Straub and Wang, 2013)
Deltaic	Ganges River delta	0.31	NA	Cited in: (Straub and Wang, 2013)
Deltaic	Mississippi River delta	0.25	NA	Cited in: (Straub and Wang, 2013)
Deltaic	Indus River delta	0.12	NA	Cited in:

				(Straub and Wang, 2013)
Deltaic	Yangtze River delta	0.09	NA	Cited in: (Straub and Wang, 2013)
Fluvial	Eocene Willwood Formation, Bighorn basin, Wyoming, U.S.A.	0.275-0.35	Biostratigraphy	(Foreman, 2014)
Fluvial	Lower Mississippi River	34-58	OSL	(Rowland et al., 2005)
Fluvial	Birch Creek, Alaska U.S.A.	6.1	OSL	(Rowland et al., 2005)
Fluvial	Middle Fly River, Papua New Guinea	2.8-7.1	OSL	(Rowland et al., 2005)
Fluvial	Rio Beni River, Bolivia	15-270	^{210}Pb	(Gautier et al., 2010)
Fluvial	Amazon floodplain	3-6	NA	Cited in: (Gautier et al., 2010)
Fluvial	Curuai floodplain	1.2-1.9	NA	Cited in: (Gautier et al., 2010)
Fluvial	Teetsa River	Uplands: 34.6 Lowlands: 16-26 High elevations: 3.3	NA	Cited in: (Gautier et al., 2010)
Fluvial	Eocene-Oligocene Horta-Gandesa alluvial system, Ebro basin, Spain	0.03-0.21	Biostratigraphy	(Jones et al., 2004)
Fluvial	Strickland River, Papua New Guinea	10-55 mean: 16	^{210}Pb	(Aalto et al., 2008)
Fluvial	Upper Columbia River, British Columbia, Canada	1.75	^{14}C	(Makaske et al., 2002)
Lacustrine	Eocene Green River Formation, Greater Green River, Uinta, and Piceance basins, Utah and Colorado, U.S.A.	0.1-1.1 Mean ~0.2	$^{40}Ar/^{39}Ar$	(Smith et al., 2008)
Deep marine	Shatsky Rise	0.003	Orbital tuning	(Bralower et al., 2014)
Deep marine	Southern ocean	0.024	Orbital tuning	(Bralower et al., 2014)

All sedimentation rates are for Quaternary accumulation unless otherwise indicated.

Table S2: Event bed or scour depth size and return interval from shelf and river depositional environments

Environment	Location	Event size (deposition is positive, erosion negative)	Approximate return interval	Citation
Shelf	Eel river shelf	10 cm	~100 yr	(Sommerfield and Nittrouer, 1999)
Shelf	Eel river shelf	<5cm	~10-20 yr	(Wiberg, 2000)
Shelf	Gulf coast	-0.3 cm	<50 yr	(Teague et al., 2006)
Shelf	Gulf coast	0.5-2m	50-100 yr	(Bentley et al., 2002; Keen et al., 2004)
Shelf	Waipaoa River margin, New Zealand	+/- 5cm	~2 yr	(Hale et al., 2014; Walsh et al., 2014)
Fluvial—over bank deposition	Yellow River	~1m deposition single event	~50 yr	(van Gelder et al., 1994)
Fluvial—over bank erosion	Yellow River	-1’s to -10’s cm	~50 yr	(van Gelder et al., 1994)
Fluvial—floodplain channels	Bighorn Basin	+/-3m	>1 kyr	(Kraus and Davies-Vollum, 2004)
Fluvial—channel	Nahal Me'arot, NW Israel	+/- 1m	~50yr	(Greenbaum and Bergman, 2006)
Fluvial—channel	Redwood Creek, California U.S.A.	+/- 1m	<5 yr	(Madej and Ozaki, 1996)
Fluvial—channel	Howgill Fells, northwest England	+/- 2m	~100 yr	(Harvey, 2007)

DOI:10.1130/G39367.1

Fluvial—avulsion	Columbia River, British Columbia, Canada	+/- 2m	800-3,000 yr	(Makaske et al., 2002)
Fluvial—avulsion	Saskatchewan River, Canada	+/- 2-3m	~600 yr	(Morozova and Smith, 2000)
Fluvial—splays	Sandover River, Australia	+/- 2 m	~50 yr	(Tooth, 2005)

4. Stochastic Sedimentation Model

We wrote a model that creates synthetic proxy records with stochastic sedimentation in the R statistical computing language, using the packages TTR and VGAM in addition to the base R library (R Core Team, 2015; Yee, 2015; Ulrich, 2016). We verified that stratigraphy built with the model reproduces the "Sadler Effect" where there is a power law relationship between sedimentation rate and the amount of time over which the sedimentation rate is calculated, with a power ~0.5 (Sadler, 1981; Sadler and Strauss, 1990; Jerolmack and Sadler, 2007).

The complete model source code and the 2,000 synthetic records we produced for this manuscript are available at https://scholarsphere.psu.edu/collections/02870v99r.

Interpretation of the synthetic records was done manually by S. Trampush. The interpretations we used for this manuscript are available at https://scholarsphere.psu.edu/collections/02870v99r.

Table S3: Model Parameters

	Model 1	Model 2	Model 3	Model 4
Number of iterations	500	500	500	500
Duration (kyr)	350	350	350	350
Scaling parameter (α)	1	0.75	1	0.75
Maximum allowed event size ($\|x_{max}\|$) (cm)	200	400	200	400
Median sediment rate ($\bar{x}$)(cm/kyr)	30	30	10	10
100 yr event (cm)	5	16	5	16
1,000 yr event (cm)	40	170	40	170
10,000 yr event (cm)	140	360	140	360

Note: Models generate sedimentation rates randomly from a double-Pareto distribution with parameters $\bar{x}$, α, and $\pm x_{max}$.

Publisher: GSA
Journal: Geology
DOI:10.1130/G39367.1

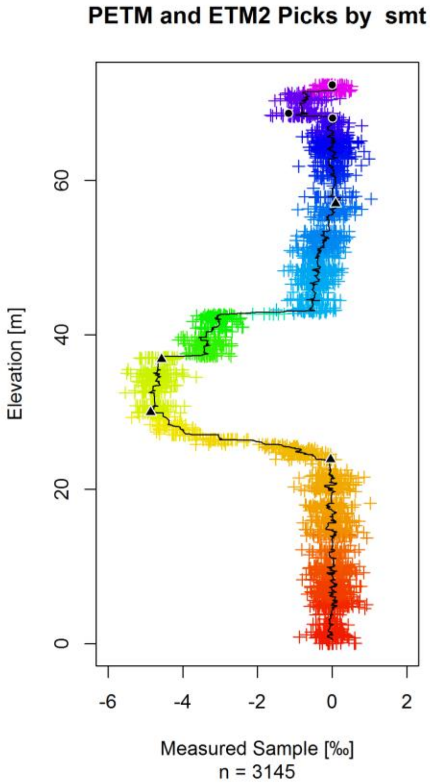

Figure S1 Example of interpretation of a synthetic record. Manual picks of the onset, peak, body, and recovery of the large event are shown by black triangles. Manual picks of the onset, peak, and recovery for the small event are shown by black circles. Criteria for the onset of both events is the point at which the moving average value of the synthetic record (black line) starts to decrease rapidly. The peak was picked as the most negative value of the moving average. Recovery is the point at which the moving average returns to the pre-excursion value. The body of the large event was defined as the last point at which the moving average is within 1‰ of the peak. For the purposes of the main text (e.g. Table 2) the duration of the recovery includes the duration of the body (see Table S3).

5. Details of Model Results and Analysis

Table S4 provides the median, 10th, and 90th percentiles of all the model (thickness, sedimentation rate, gap size, etc.) and interpreted parameters (event magnitude, duration, shape, etc.). Figure S2 shows the full distributions for every parameter we measured. Table S5 shows statistics of how many annual events were preserved, how many were removed because of hiatuses, and how many were removed due to erosion.

Table S4: Complete Model Results

	Model 1: High Sedimentation, Low variability	Model 2: High Sedimentation, High Variability	Model 3: Low Sedimentation, Low Variability	Model 4: Low Sedimentation, High Variability
All Synthetic Records				
Thickness of synthetic section (m) (input = 105 m for model 1 & 2 or 35 m for model 3 & 4)	110 (78-141)	130 (49-213)	44 (16-75)	82 (20-174)
Total time represented in section (kyr)	346	313	319	250

Publisher: GSA
Journal: Geology
DOI:10.1130/G39367.1

(input = 350 kyr)	(320-350)	(143-349)	(12-349)	(40-347)
Generalized sedimentation rate* (cm/kyr) (input = 10 or 30 cm/kyr)	31 (22-40)	37 (14-61)	13 (5-21)	23 (6-50)
Measured sedimentation rate** (cm/kyr) (input = 10 or 30 cm/kyr)	33 (23-42)	48 (23-79)	16 (7-28)	42 (19-94)
Maximum gap in the record (kyr)	43 (27-84)	91 (35-191)	81 (33-175)	86 (15-205)
Preserved record of large event	100% (500)	88% (438)	87% (434)	69% (344)
Preserved a record of small event	89% (445)	53% (265)	58% (291)	44% (222)
Preserved a record of the small event only	0% (0)	5% (27)	6% (29)	56% (11%)
Preserved a record of both large and small events	89% (445)	48% (238)	52% (262)	33% (166)
Large Event Records				
Measured Sedimentation rate** (cm/kyr) (input = 10 or 30 cm/kyr)	33 (23 – 42)	48 (23 – 79)	16 (8 – 25)	38 (20 – 69)
Apparent Total Duration (kyr) (input = 200 kyr)	193 (141-236)	165 (81-236)	176 (87-255)	154 (68-240)
Apparent Magnitude (‰) (input = -4.7 to -5.2 ‰)	-5.0 (-5.2 - -4.5)	-4.6 (-5.2 - -2.2)	-4.7 (-5.2 - -2.6)	-4.1 (-5.1 - -1.5)
Apparent Onset Duration (kyr) (input = 20 kyr)	19 (3 - 46)	15 (2-57)	16 (2-53)	10 (2-58)
Apparent Recovery Duration (kyr) (input = 180 kyr)	171 (116-215)	131 (51-215)	138 (51-224)	117 (40-210)
Small Event Records				
Measured Sedimentation rate** (cm/kyr) (input = 10 or 30 cm/kyr)	33 (24-42)	48 (22-78)	18 (11-28)	51 (27-85)
Apparent Total Duration (kyr) (input = 40 kyr)	40 (17-69)	44 (18-94)	47 (20-87)	44 (17-90)
Apparent Magnitude (‰) (input = -0.7 to 1.3 ‰)	-1.1 (-1.3 - -0.7)	-1.1 (-1.3- -0.7)	-1.1 (-1.3- -0.7)	-1.1 (-1.3- -0.8)
Apparent onset duration (kyr) (input = 4 kyr)	4 (1-10)	5 (1-14)	5 (2-17)	4 (1-15)
Apparent recovery duration (kyr) (input = 36 kyr)	35 (11-64)	37 (12 -83)	36 (15-81)	37 (11-79)
Note: Table reflects median values calculated with all 500 synthetic records in each model. Parentheses contain 10th and 90th percentiles.				

Table S5: Annual events preserved, eroded, or not deposited

	Model 1	Model 2	Model 3	Model 4
Number of preserved annual events	3,993 (2,784 – 5,182)	1,347 (526 – 2,264)	1,243 (427 – 2,070)	742 (178 – 1,590)
Number of annual events with deposition between 0 and 0.5 mm	68,198 (67,978 – 68,498)	52,817 (52,525 – 53,029)	68,257 (67,965 – 68,516)	52,763 (52,522 – 53,090)
Number of annual events removed by erosion	277,779 (276,456 – 278909)	295,879 (294,894 – 296,686)	280,559 (279,572 – 281,395)	296,429 (295,569 – 297,001)
Note: Table reflects median values calculated with all 500 synthetic records in each model. Parentheses contain 10th and 90th percentiles.				

Additionally, we used these distributions to evaluate whether climate signal characteristics estimated from individual records (e.g., total duration and duration of onset) were significantly different if a specific local age model was used instead of a generalized age model. For each record the measured local sedimentation

Publisher: GSA
Journal: Geology
DOI:10.1130/G39367.1
rate was obtained by dividing the thickness of the record by the time span between the age of the lowermost and upper most beds preserved. This is analogous to using biozones at the base and top of a section to estimate local sedimentation rates. In contrast, the generalized age model is simply the total record thickness divided by 350 kyr. This difference had little influence on the estimated duration, magnitude, or shape of the large or small event (Figure S2). The only exception to this apparent insensitivity to sedimentation rate was the small number of records which only preserved the small event: because these records only preserved the last ~100 kyr, the generalized sedimentation rate was much smaller than the measured rate, which made the duration of the small event appear excessively long. Table 1 and Table S4 event statistics were made with the measured local sedimentation rate, not the general sedimentation rate.

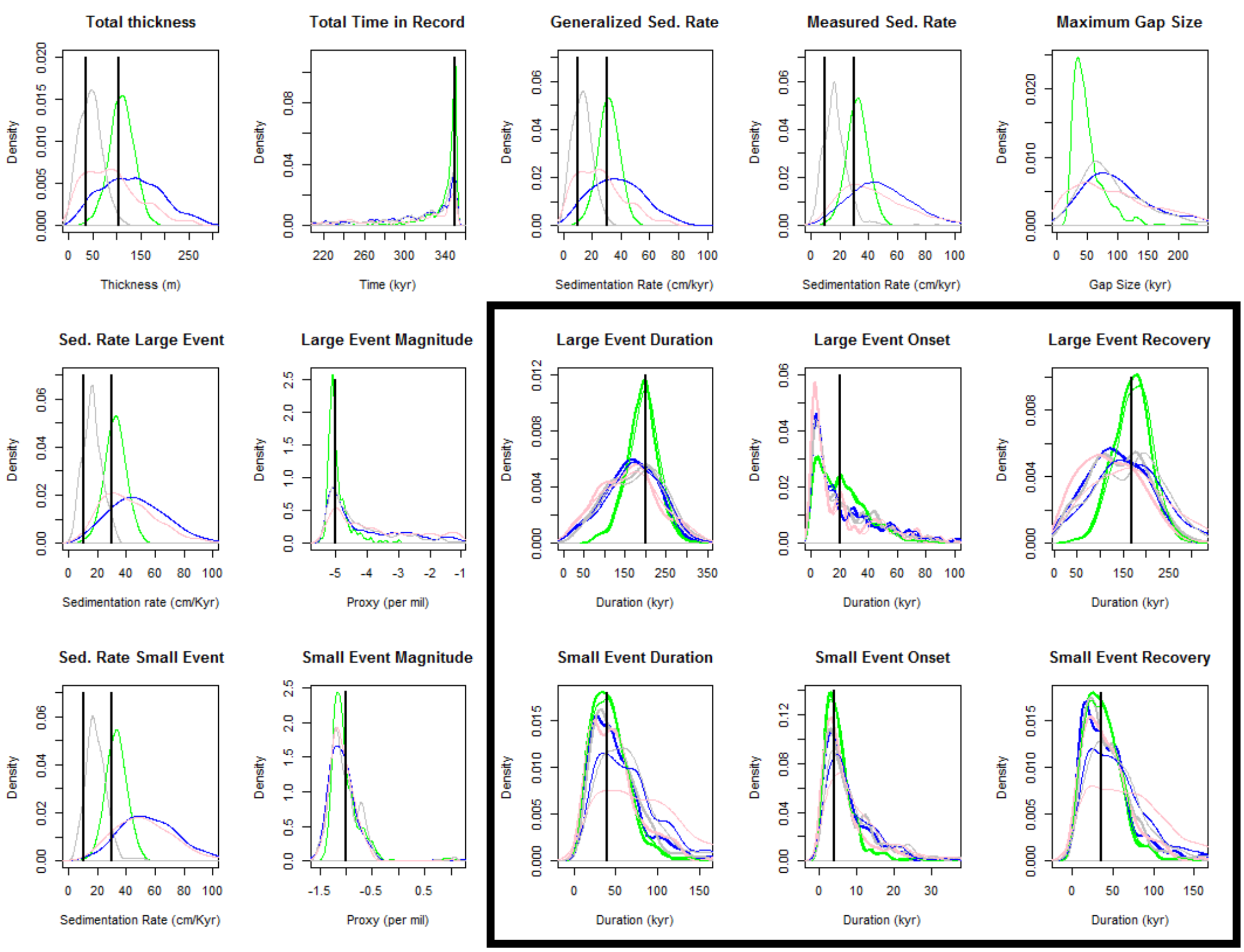

Figure S2: Kernel density estimates of the distributions of the parameters in Table 2. Colors are the same as in Figure 3: green is Model 1 (high sedimentation, low sediment variability), blue is Model 2 (high sedimentation, high sedimentation variability), grey is Model 3 (low sedimentation, low sedimentation variability), and pink is Model 4 (low sedimentation, high sedimentation variability). The black box shows the parameters that were measured using the measured sedimentation rate (thick lines) and the interval sedimentation rate (thin lines). The estimates are essentially identical for both sedimentation rates, with the exception of the records which only preserved the small event.

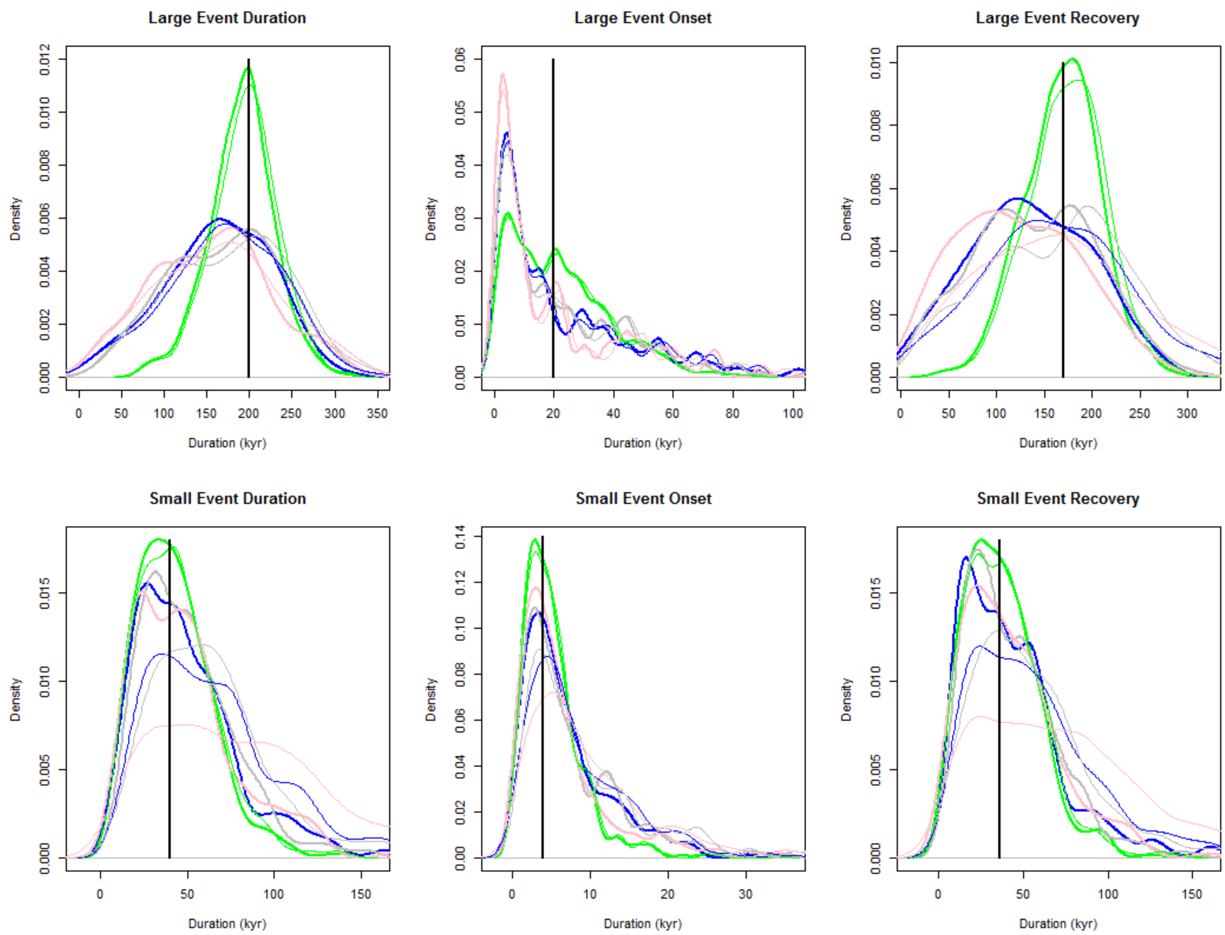

Figure S3: Detail of the 6 event parameters kernel density estimate (black box Figure S1) calculated by the measured sedimentation rate (thick lines) and interval sedimentation rate (thin lines).

5.1 Appearance of a Body in the Large Event

In addition to the parameters reported in Table 1, we also measured the duration of any apparent body in synthetic proxy records (Table S6). A body was defined as an extended excursion, i.e. a thick or protracted period of proxy values within 1‰ of the peak excursion (e.g., second Model 2 record of figure 3).

Publisher: GSA
Journal: Geology
DOI:10.1130/G39367.1

Table S6: Duration of large climate events in records with excursion bodies.

	Model 1: High Sedimentation, Low variability	Model 2: High Sedimentation, High Variability	Model 3: Low Sedimentation, Low Variability	Model 4: Low Sedimentation, High Variability
Apparent Body Duration (kyr) (input = 1 yr)	36 (12-82)	39 (8-103)	43 (8 - 112)	48 (7-131)
Apparent Recovery Duration (kyr) (input = 180 kyr)	132 (70-183)	81 (5-167)	84 (3-163)	64 (6-160)
Apparent Recovery + Body Duration (kyr) (input = 180 kyr)	171 (116-215)	131 (51-215)	138 (51-224)	117 (40-210)

5.2 Small Event Preservation

The small event was more likely to be preserved than might be expected given its short duration. This is because the small event occurs at the top of the section (late in the model succession) there is less opportunity for it to be removed by large erosion events. It is very difficult to preserve the small event if it is placed earlier in the model succession. Additionally, because the 1‰ excursion is small relative to the noise of the proxy system (std. dev. 0.3‰), when the small event was identifiable it was likely to be slightly overestimated in magnitude and duration, and its shape tended to be well represented since preservation only occurred if there was a run of thick beds deposited in succession.

5.3 Thickness of Deposit and Event Preservation Probability

We assessed whether thicker sections had a higher probability of preservation (Figure S4, Table S7). We found that records that preserved either the large or small event were slightly thicker than the distribution of the entire population of synthetic records. However, many thin records preserved one or both events, and many thick records failed to preserve either events.

Publisher: GSA
Journal: Geology
DOI:10.1130/G39367.1

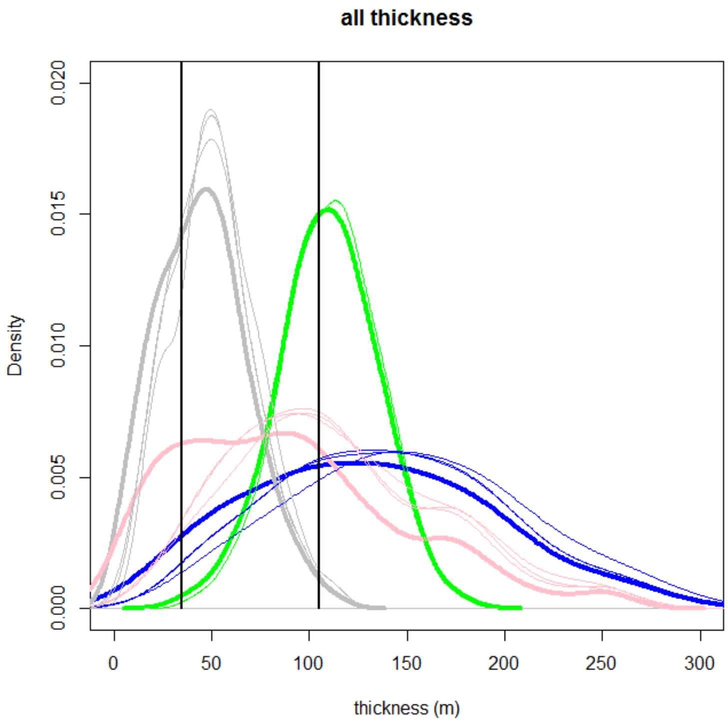

Figure S4: Kernel density estimates of the thickness of all records (thick lines) and records which preserved one or both of the events (thin lines) from Models 1 (green), 2 (blue), 3 (grey), and 4 (pink).

Table S7: Thickness of records which preserved one, both, or neither events

	Model 1: High Sedimentation, Low variability	Model 2: High Sedimentation, High Variability	Model 3: Low Sedimentation, Low Variability	Model 4: Low Sedimentation, High Variability
Thickness all sections:	110 (78-141)	130 (49-213)	44 (16-75)	82 (20-174)
Thickness if large event preserved	110 (78-141)	139 (64-217)	49 (23-77)	104 (47-184)
Thickness if small event preserved	112 (80-143)	148 (71-235)	52 (24-82)	110 (51-191)
Thickness if both events preserved	112 (80-143)	158 (89-241)	54 (29-83)	129 (74-198)
Thickness if neither event preserved	NA	32 (13-62) (n=35)	9 (2-19) (n=37)	22 (5-53) (n=100)

Parentheses contain the 10^{th} to 90^{th} percentiles.

6. Probability of Accurately Reconstructing the Input Signal

To gauge and compare how accurately records from different models reconstructed the input climate signal, we used the age model created with the measured local sedimentation rate and counted the number of interpreted records that were within 50, 20, and 10% of the magnitude, duration, onset duration, and recovery duration of the input signal (Table S8). The recovery duration includes the duration of the body if one appeared in a record.

Table S8: Number of records that estimate the magnitude, duration, duration of onset, and duration of recovery within 50, 20, and 10% of the input large climate event. Input large-event values shown in parentheses.

Parameter	Model 1 (n=500)	Model 2 (n=438)	Model 3 (n=434)	Model 4 (n=344)
Magnitude (input = -5‰)				
50% error (-7.7 to -2.5‰):	499 (100%)	380 (87%)	395 (91%)	267 (78%)
20% error (-6 to -4‰):	484 (97%)	281 (64%)	303 (70%)	180 (52%)
10% error (-5.5 to – 4.5‰):	449 (90%)	238 (54%)	246 (57%)	130 (38%)
Duration (input = 200 kyr)				
50% error (100 to 300 kyr):	469 (94%)	228 (52%)	241 (56%)	125 (36%)
20% error (160 to 240 kyr):	348 (70%)	127 (29%)	120 (28%)	65 (19%)
10% error (180 to 220 kyr):	203 (41%)	52 (12%)	71 (16%)	36 (10%)
Onset duration (input = 20 kyr)				
50% error (10 to 30 kyr):	211 (42%)	77 (18%)	84 (19%)	30 (9%)
20% error (16 to 24 kyr):	85 (17%)	26 (6%)	36 (8%)	24 (7%)
10% error (18 to 22 kyr):	58 (12%)	15 (3%)	17 (4%)	14 (4%)
Could not be determined:	21 (4%)	163 (37%)	141 (32%)	175 (51%)
Recovery (input = 180 kyr)				
50% error (85 to 255 kyr):	482 (96%)	326 (74%)	327 (75%)	226 (66%)
20% error (136 to 204 kyr):	307 (61%)	142 (32%)	145 (33%)	104 (30%)
10% error (153 to 187 kyr):	175 (35%)	69 (16%)	81 (19%)	52 (15%)
Total within error for magnitude, total duration, and onset duration				
50% error:	207 (41%)	55 (13%)	65 (15%)	27 (8%)
20% error:	59 (12%)	15 (3%)	15 (3%)	6 (2%)
10% error:	25 (5%)	3 (0.7%)	3 (0.7%)	1 (0.3%)

7. Ensemble Records of Models (Figure 4A & B)

Multiple ensemble records were constructed to evaluate how accurately aggregate records reconstruct the input climate signal. We generated ensemble records for the best preserved (Model 1) and worst preserved (Model 4) models using the median of 15 randomly selected individual records that preserve the large event and where the onset and recovery of the large event can be measured. Individual records in the ensembles were datumed on the onset of the excursion and used the measured local sedimentation rate for an age model. Example ensemble records are shown in Figure 4 A & B. For each scenario we generated 500 unique ensemble records. Age models for the records were made using the measured sedimentation rate. The ensemble record was made by taking the median of all 15 records of the magnitude, duration, onset duration, and recovery duration. We then counted how many ensembles were within 50, 20, and 10% of the input signal (Table S9).

Table S9: Error of ensembles of 15 random records

Parameter	Model 1 (Count of 500 ensembles of 15 records)	Model 4 (Count of 500 ensembles of 15 records)
Magnitude		
50% error:	500 (100%)	500 (100%)
20% error:	500 (100%)	464 (93%)
10% error:	500 (100%)	305 (61%)
Duration		
50% error:	500 (100%)	493 (99%)
20% error:	499 (100%)	224 (45%)
10% error:	422 (84%)	63 (13%)
Onset		
50% error:	473 (95%)	226 (45%)
20% error:	266 (53%)	134 (27%)
10% error:	185 (37%)	68 (13%)
Recovery		
50% error:	500 (100%)	477 (95%)
20% error:	493 (99%)	230 (46%)
10% error:	425 (85%)	107 (21%)
Total within error for magnitude, total duration, and onset duration:		
50% error:	473 (95%)	225 (45%)
20% error:	265 (53%)	72 (14%)
10% error:	163 (33%)	9 (2%)

Table S10: Medians and range in parentheses of ensemble curves used in Figure 4C.

Parameter	Ensemble in Fig4A	Ensemble in Fig4B	Ensemble in Fig4C
Magnitude	-5.1‰ (-4.6 to -5.3‰)	-4.0‰ (-3.1 to -5.2‰)	-2.5‰ (-1 to -5‰)
Total duration	198 kyr (119 to 271 kyr)	195 kyr (43 to 290 kyr)	185 kyr (35 to 600 kyr)
Onset duration	18 kyr (1.4 to 57 kyr)	22 kyr (0.4 to 118 kyr)	10 kyr (5 to 50 kyr)

Parentheses contain the min/max values for each parameter.

8. PETM Ensemble (Figure 4C)

The ensemble of PETM curves in Figure 4C was made using the same 15 records in the compilation above. We used the elevation of the onset (as defined by the original authors), a long term sedimentation rate calculated using the author-reported sedimentation rate, biostratigraphy, or subsidence rates. We also subtracted the individual record's pre-CIE $\delta^{13}C_{org}$ value to compare a relative $\delta^{13}C_{org}$ offset (Table S11). We then compared the amount of variability in estimates of the magnitude, duration, and onset duration of the PETM individual records to the values estimated from the ensemble record (Table S12). Finally, we assessed the sensitivity of the PETM ensemble to the age models derived from the linear sedimentation rates by randomly changing 1/3 of the sedimentation rates by a factor of 2 (Figure S5 A-J, Table S12). We also assess what would happen if the sedimentation rate for the northern Spain records were all too low, or if the Wyoming records were all too high (Figure S5J & L, Table S12). We find that the magnitude, duration, onset duration, and overall shape are relatively insensitive to sedimentation rate errors within a factor of two.

While it has been proposed that sedimentation rate increased dramatically across the PETM, the amount of increase and the timing of the increase is not clear (Schmitz et al., 2001; Schmitz and Pujalte, 2007; Kopp et al., 2009; McInerney and Wing, 2011; Foreman et al., 2012; Garel et al., 2013). Additionally several studies have suggested that variability in sedimentation would also have increased during this time; our model results show that if sedimentation rates increase commensurately with variability in sedimentation, the net effect is no change on signal preservation. Since we are using the PETM as a heuristic example, and not trying to precisely define the true PETM signal, we ignore this complexity. More complicated sedimentation rate age models would be more appropriate if a more precise ensemble of the PETM is desired.

Table S11: Bulk organic carbon isotope records used in ensemble Figure 4C.

Name	Location	Depositional Environment	Sedimentation Rate* (cm/kyr)	Pre-CIE $\delta^{13}C_{org}$ value (‰)	Citations
Highway 16	Bighorn Basin, Wyoming, USA	Fluvial	20	-24.5	Data: (Baczynski et al., 2013) Sedimentation rate: (Secord et al., 2010)
CAB10	Bighorn Basin, Wyoming, USA	Fluvial	20	-24.0	Data: (Baczynski et al., 2013) Sedimentation rate: (Secord et al., 2010)
Big Red Spit	Bighorn Basin, Wyoming, USA	Fluvial	20	-25.0	Data: (Baczynski et al., 2013) Sedimentation rate: (Secord et al., 2010)
North Butte	Bighorn Basin, Wyoming, USA	Fluvial	20	-25.0	Data: (Baczynski et al., 2013) Sedimentation rate: (Secord et al., 2010)
Polecat Bench	Bighorn Basin, Wyoming, USA	Fluvial	40	-24.5	Data: (Magioncalda et al., 2004) Sedimentation rate: (Clyde, 1997)
De Beque	Piceance Basin, Colorado, USA	Fluvial	27.5	-23.5	Data and sedimentation rate: (Foreman et al., 2012)
Lodo Gulch	Californian margin	Marginal marine	20	-23.5	Data and sedimentation rate: (John et al., 2008)
Tumey Gulch	Californian margin	Marginal marine	5	-24.0	Data and sedimentation rate: (John et al., 2008)
Claret	Tremp–Graus basin, Northern Spain	Fluvial	20	-23.5	Data: (Manners et al., 2013) Sedimentation rate: (Torricelli et al., 2006)
Tendrui	Tremp–Graus basin, Northern Spain	Fluvial	20	-25.0	Data: (Manners et al., 2013) Sedimentation rate: (Torricelli et al., 2006)
Campo	Tremp–Graus basin, Northern Spain	Transitional mixed shallow marine and continental	2	-26.5	Data: (Manners et al., 2013) Sedimentation rate: (Molina et al., 2000) and (Vandenberghe et al., 2012)
Esplugafreda	Tremp–Graus basin, Northern Spain	Fluvial	20	-23.0	Data: (Manners et al., 2013) Sedimentation rate: (Torricelli et al., 2006)
Ermua	Basque–Cantabrian basin, Northern Spain	Marine; “base-of-slope-apron”	15	-24.0	Data: (Manners et al., 2013) Sedimentation rate**:

					(Gomez et al., 2002; Schmitz and Pujalte, 2003)
Zumaia	Basque–Cantabrian basin, Northern Spain	Bathyal marine/Marine turbidites	5	-25.0	Data: (Manners et al., 2013) Sedimentation rate***: (Gomez et al., 2002)
IODP 1172	Southern Ocean	Marginal marine/deltaic	0.57	-26.5	Data and sedimentation rate: (Sluijs et al., 2011)

*Sedimentation rate refers to the median value measured across the PETM
**Inferred from the subsidence rate in the Basque-Cantabrian basin and from the relative thickness of the correlations between Ermua and Zumaia (i.e. Ermua is ~3 times as thick as Zumaia, therefore sedimentation rate should be ~3 times as rapid)
***Inferred from subsidence rate in the Basque-Cantabrian basin

Table S12: Sensitivity of Ensembles to Sedimentation Rate

Name	A (Figure 4C)	B	C	D	E	F	G	H	I	J	K	L
Sedimentation Rates												
Highway 16	20	10	20	20	40	20	20	40	40	20	20	10
CAB10	20	20	10	20	40	10	20	10	10	20	20	10
Big Red Spit	20	40	20	40	20	20	20	20	20	20	20	10
North Butte	20	20	20	20	20	20	40	20	20	40	20	10
Polecat Bench	40	40	20	80	40	20	40	20	40	40	40	20
De Beque	27.5	27.5	27.5	27.5	13.75	27.5	27.5	27.5	55	27.5	27.5	27.5
Lodo Gulch	20	20	20	20	20	40	10	20	20	10	20	20
Tumey Gulch	5	5	10	5	5	5	2.5	5	5	5	5	5
Claret	20	20	40	20	40	20	20	20	40	20	40	20
Tendrui	20	10	20	40	20	20	20	20	20	20	40	20
Campo	2	2	4	2	2	4	2	2	2	2	4	2
Esplugafreda	20	20	20	40	20	20	20	20	40	20	40	20
Ermua	15	30	15	15	15	30	15	30	15	30	30	15
Zumaia	5	5	5	5	10	5	2.5	10	5	2.5	10	5
IODP 1172	0.57	1.14	0.57	0.57	0.57	0.57	0.57	0.57	0.57	0.57	0.57	0.57
Ensemble values												
Magnitude (‰)	2.5	2.8	2.7	2.5	2.4	2.7	3.0	2.5	2.6	2.8	2.7	2.7
Total Duration (kyr)	190	180	220	190	220	210	210	190	220	190	170	220
Onset duration (kyr)	10	10	10	6	6	10	8	6	7	10	5	15

Red boxes: sedimentation rate decreased by factor of 2, blue boxes: sedimentation rate increased by a factor of 2

Publisher: GSA
Journal: Geology
DOI:10.1130/G39367.1

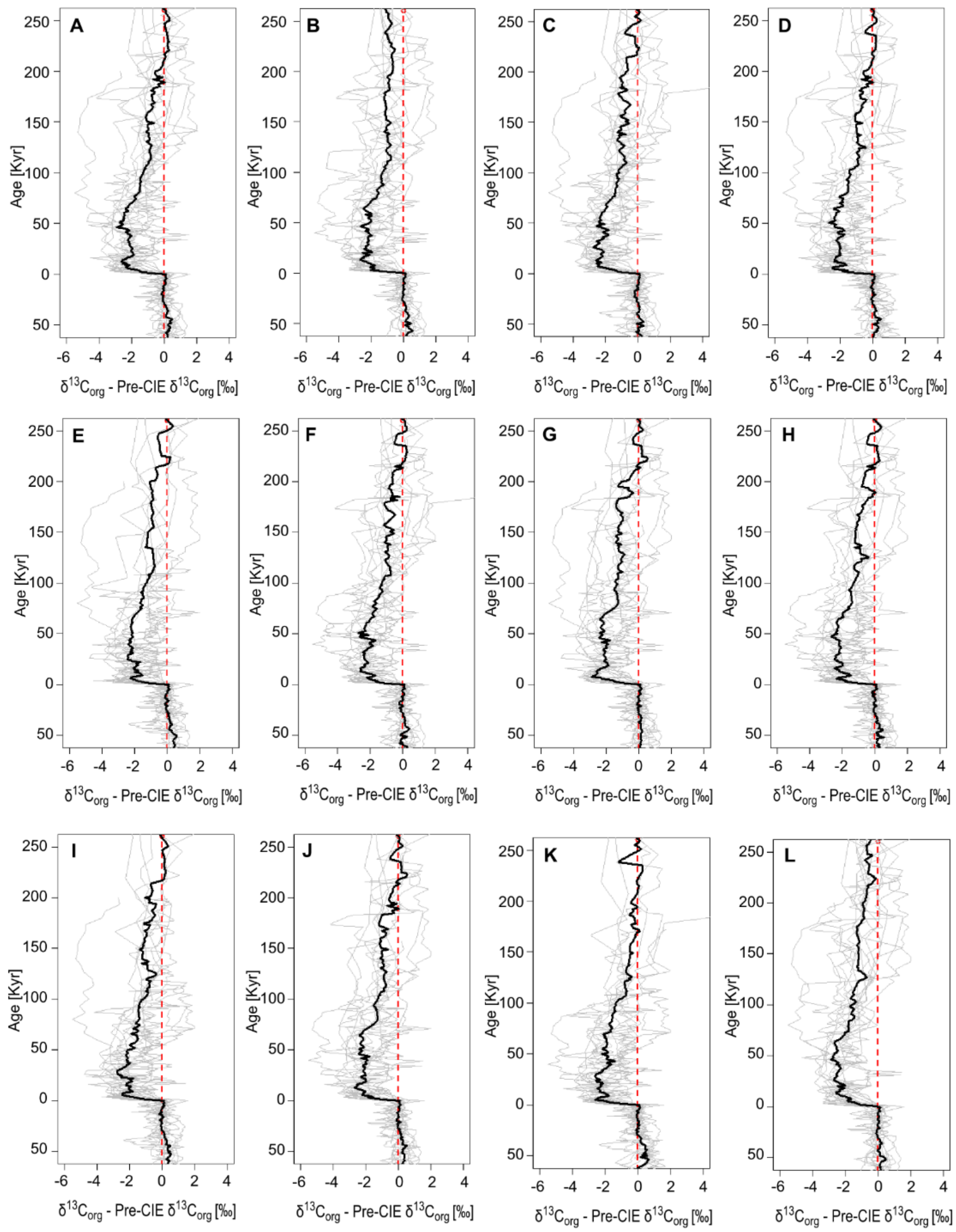

Figure S5: Sensitivity of PETM ensemble to factor of 2 errors in sedimentation rate. Sedimentation rates used for each ensemble in Table S9.

10. References

Aalto, R., Lauer, J.W., and Dietrich, W.E., 2008, Spatial and temporal dynamics of sediment accumulation and exchange along Strickland River floodplains (Papua New Guinea) over decadal-to-centennial timescales: Journal of Geophysical Research: Earth Surface, v. 113, p. 1–22, doi: 10.1029/2006JF000627.

Baczynski, A.A., McInerney, F.A., Wing, S.L., Kraus, M.J., Jonathan, I., Boyer, D.M., Secord, R., Morse, P.E., Fricke, H.C., Bloch, J.I., Boyer, D.M., Secord, R., Morse, P.E., and Fricke, H.C., 2013, Chemostratigraphic implications of spatial variation in the Paleocene-Eocene Thermal Maximum carbon isotope excursion, SE Bighorn Basin, Wyoming: Geochemistry, Geophysics, Geosystems, v. 14, no. 10, p. 4133–4152, doi: 10.1002/ggge.20265.

Bentley, S.J., Keen, T.R., Blain, C.A., and Chad Vaughan, W., 2002, The origin and preservation of a major hurricane event bed in the northern Gulf of Mexico: Hurricane Camille, 1969: Marine Geology, v. 186, no. 3–4, p. 423–446, doi: 10.1016/S0025-3227(02)00297-9.

Bralower, T.J., Meissner, K.J., Alexander, K., and Thomas, D.J., 2014, The dynamics of global change at the Paleocene-Eocene thermal maximum: A data-model comparison: Geochemistry, Geophysics, Geosystems, v. 15, p. 3830–3848, doi: 10.1002/2014GC005474.

Carlin, J.A., and Dellapenna, T.M., 2014, Event-Driven Deltaic Sedimentation on a Low-Gradient, Low-Energy Shelf: The Brazos River Subaqueous Delta, Northwestern Gulf of Mexico: Marine Geology, v. 353, p. 21–30, doi: 10.1016/j.margeo.2014.03.017.

Clyde, W.C., 1997, Stratigraphy and mammalian paleontology of the McCulluogh Peaks, Northern Bighorn Basin, Wyoming: Implications for biochronology, basin development, and community reorganization across the Paleocene-Eocene Boundary, Ph.D. Dissertation: The University of Michigan, 1-271 p.

Ferré, B., Sherwood, C.R., and Wiberg, P.L., 2010, Sediment transport on the Palos Verdes shelf, California: Continental Shelf Research, v. 30, p. 761–780, doi: 10.1016/j.csr.2010.01.011.

Foreman, B.Z., 2014, Climate-driven generation of a fluvial sheet sand body at the Paleocene-Eocene boundary in north-west Wyoming (USA): Basin Research, v. 26, no. 2, p. 225–241, doi: 10.1111/bre.12027.

Foreman, B.Z., Heller, P.L., and Clementz, M.T., 2012, Fluvial response to abrupt global warming at the Palaeocene/Eocene boundary: Nature, v. 490, no. 7422, p. 92–95, doi: 10.1038/nature11513.

Garel, S., Schnyder, J., Jacob, J., Dupuis, C., Boussafir, M., Le Milbeau, C., Storme, J.Y., Iakovleva, A.I., Yans, J., Baudin, F., Fléhoc, C., and Quesnel, F., 2013, Paleohydrological and paleoenvironmental changes recorded in terrestrial sediments of the Paleocene-Eocene boundary (Normandy, France): Palaeogeography, Palaeoclimatology, Palaeoecology, v. 376, p. 184–199, doi: 10.1016/j.palaeo.2013.02.035.

Gautier, E., Brunstein, D., Vauchel, P., Jouanneau, J.M., Roulet, M., Garcia, C., Guyot, J.L., and Castro, M., 2010, Channel and floodplain sediment dynamics in a reach of the tropical meandering Rio Beni (Bolivian Amazonia): Earth Surface Processes and Landforms, v. 35, no. September, p. 1838–1853, doi: 10.1002/esp.2065.

van Gelder, A., van den Berg, J.H., Cheng, G., and Xue, C., 1994, Overbank and channelfill deposits of the modern Yellow River delta: Sedimentary Geology, v. 90, p. 293–305, doi: 10.1016/0037-0738(94)90044-2.

Gomez, M., Verges, J., and Riaza, C., 2002, Inversion tectonics of the northern margin of the Basque Cantabrian Basin: Bulletin de la Societe Geologique de France, v. 173, no. 5, p. 449–459, doi: 10.2113/173.5.449.

Greenbaum, N., and Bergman, N., 2006, Formation and evacuation of a large gravel-bar deposited during a major flood in a Mediterranean ephemeral stream, Nahal Me'arot, NW Israel: Geomorphology, v. 77, p. 169–186, doi: 10.1016/j.geomorph.2006.01.016.

Hale, R.P., Ogston, A.S., Walsh, J.P., and Orpin, A.R., 2014, Sediment transport and event deposition on the Waipaoa River Shelf, New Zealand: Continental Shelf Research, v. 86, p. 52–65, doi: 10.1016/j.csr.2014.01.009.

Harvey, A.M., 2007, Differential recovery from the effects of a 100-year storm: Significance of long-term hillslope-channel coupling; Howgill Fells, northwest England: Geomorphology, v. 84, p. 192–208, doi: 10.1016/j.geomorph.2006.03.009.

Jerolmack, D.J., and Sadler, P., 2007, Transience and persistence in the depositional record of continental margins: Journal of Geophysical Research: Earth Surface, v. 112, p. 1–14, doi: 10.1029/2006JF000555.

John, C.M., Bohaty, S.M., Zachos, J.C., Sluijs, A., Gibbs, S., Brinkhuis, H., and Bralower, T.J., 2008, North American continental margin records of the Paleocene-Eocene thermal maximum: Implications for global carbon and hydrological cycling: Paleoceanography, v. 23, p. 1–20, doi: 10.1029/2007PA001465.

Jones, M.A., Heller, P.L., Roca, E., Garcés, M., and Cabrera, L., 2004, Time lag of syntectonic sedimentation across an alluvial basin: Theory and example from the Ebro Basin, Spain: Basin Research, v. 16, p. 467–488, doi: 10.1111/j.1365-2117.2004.00244.X.

Keen, T.R., Bentley, S.J., Chad Vaughan, W., and Blain, C.A., 2004, The generation and preservation of multiple hurricane beds in the northern Gulf of Mexico: Marine Geology, v. 210, no. 1–4, p. 79–105, doi: 10.1016/j.margeo.2004.05.022.

Kopp, R.E., Schumann, D., Raub, T.D., Powars, D.S., Godfrey, L. V., Swanson-Hysell, N.L., Maloof, A.C., and Vali, H., 2009, An Appalachian Amazon? Magnetofossil evidence for the development of a tropical river-like system in the mid-Atlantic United States during the Paleocene-Eocene thermal maximum: Paleoceanography, v. 24, no. 4, p. 1–17, doi: 10.1029/2009PA001783.

Kraus, M.J., and Davies-Vollum, K.S., 2004, Mudrock-dominated fills formed in avulsion splay channels: Examples from the Willwood Formation, Wyoming: Sedimentology, v. 51, p. 1127–1144, doi: 10.1111/j.1365-3091.2004.00664.x.

Lewis, R.C., Coale, K.H., Edwards, B.D., Marot, M., Douglas, J.N., and Burton, E.J., 2002, Accumulation rate and mixing of shelf sediments in the Monterey Bay National Marine Sanctuary: Marine Geology, v. 181, no. 1–3, p. 157–169, doi: 10.1016/S0025-3227(01)00265-1.

Madej, M.A., and Ozaki, V., 1996, Channel response to sediment wave propagation and movement, Redwood Creek, California, USA: Earth Surface Processes and Landforms, v. 21, no. 10, p. 911–927, doi: 10.1002/(SICI)1096-9837(199610)21:10<911::AID-ESP621>3.0.CO;2-1.

Magioncalda, R., Dupuis, C., Smith, T., Steurbaut, E., and Gingerich, P.D., 2004, Paleocene-Eocene carbon isotope excursion in organic carbon and pedogenic carbonate: Direct comparison in a continental stratigraphic section: Geology, v. 32, no. 7, p. 553–556, doi: 10.1130/G20476.1.

Makaske, B., Smith, D.G., and Berendsen, H.J.A., 2002, Avulsions, channel evolution and floodplain sedimentation rates of the anastomosing upper Columbia River, British Columbia, Canada: Sedimentology, v. 49, no. 5, p. 1049–1071, doi: 10.1046/j.1365-3091.2002.00489.x.

Manners, H.R., Grimes, S.T., Sutton, P.A., Domingo, L., Leng, M.J., Twitchett, R.J., Hart, M.B., Dunkley Jones, T., Pancost, R.D., Duller, R., and Lopez-Martinez, N., 2013, Magnitude and profile of organic carbon isotope records from the Paleocene-Eocene Thermal Maximum: Evidence from northern Spain: Earth and Planetary Science Letters, v. 376, p. 220–230, doi: 10.1016/j.epsl.2013.06.016.

McInerney, F.A., and Wing, S.L., 2011, The Paleocene-Eocene Thermal Maximum: A Perturbation of Carbon Cycle, Climate, and Biosphere with Implications for the Future: Annual Review of Earth and Planetary Sciences, v. 39, no. 1, p. 489–516, doi: 10.1146/annurev-earth-040610-133431.

Molina, E., Angori, E., Arenillas, I., Monechi, S., and Schmitz, B., 2000, Integrated stratigraphy across the Paleocene/Eocene boundary at Campo, Spain: GFF, v. 122, no. 1, p. 106–107, doi: 10.1080/11035890001221106.

Morozova, G.S., and Smith, N.D., 2000, Holocene avulsion styles and sedimentation patterns of the Saskatchewan River, Cumberland Marshes, Canada: Sedimentary Geology, v. 130, no. 1–2, p. 81–105, doi: 10.1016/S0037-0738(99)00106-2.

R Core Team, 2015, R: A Language and Environment for Statistical Computing:

Rose, L.E., and Kuehl, S.A., 2010, Recent sedimentation patterns and facies distribution on the Poverty Shelf, New Zealand: Marine Geology, v. 270, no. 1–4, p. 160–174, doi: 10.1016/j.margeo.2009.10.020.

Rowland, J.C., Lepper, K., Dietrich, W.E., Wilson, C.J., and Sheldon, R., 2005, Tie channel sedimentation rates, oxbow formation age and channel migration rate from optically stimulated luminescence (OSL) analysis of floodplain deposits: Earth Surface Processes and Landforms, v. 30, p. 1161–1179, doi: 10.1002/esp.1268.

Sadler, P., 1981, Sediment accumulation rates and the completeness of stratigraphic sections: Journal of Geology, v. 89, p. 569–584.

Sadler, P.M., and Strauss, D.J., 1990, Estimation of completeness of stratigraphical sections using empirical data and theoretical models: Journal of the Geological Society, London, v. 147, p. 471–485.

Schmitz, B., and Pujalte, V., 2007, Abrupt increase in seasonal extreme precipitation at the Paleocene-Eocene boundary: Geology, v. 35, no. 3, p. 215–218, doi: 10.1130/G23261A.1.

Schmitz, B., and Pujalte, V., 2003, Sea-level, humidity, and land-erosion records across the initial Eocene thermal maximum from a continental-marine transect in northern Spain: Geology, v. 31, no. 8, p. 689–692, doi: 10.1130/G19527.1.

Schmitz, B., Pujalte, V., and Núñez-Betelu, K., 2001, Climate and sea-level perturbations during the Initial Eocene Thermal Maximum: Evidence from siliciclastic units in the Basque basin (Ermua, Zumaia and Trabakua Pass), northern Spain: Palaeogeography, Palaeoclimatology, Palaeoecology, v. 165, no. 3–4, p. 299–320, doi: 10.1016/S0031-0182(00)00167-X.

Secord, R., Gingerich, P.D., Lohmann, K.C., and Macleod, K.G., 2010, Continental warming preceding the Palaeocene-Eocene thermal maximum.: Nature, v. 467, no. 7318, p. 955–958, doi: 10.1038/nature09441.

Self-Trail, J.M., Powars, D.S., Watkins, D.K., and Wandless, G.A., 2012, Calcareous nannofossil assemblage changes across the Paleocene–Eocene Thermal Maximum: Evidence from a shelf setting: Marine Micropaleontology, v. 92–93, p. 61–80, doi: 10.1016/j.marmicro.2012.05.003.

Sluijs, A., Bijl, P.K., Schouten, S., Röhl, U., Reichart, G.J., and Brinkhuis, H., 2011, Southern ocean warming, sea level and hydrological change during the Paleocene-Eocene thermal maximum: Climate of the Past, v. 7, no. 1, p. 47–61, doi: 10.5194/cp-7-47-2011.

Sluijs, a., and Brinkhuis, H., 2009, A dynamic climate and ecosystem state during the Paleocene-Eocene Thermal Maximum – inferences from dinoflagellate cyst assemblages at the New Jersey Shelf: Biogeosciences Discussions, v. 6, no. 3, p. 5163–5215, doi: 10.5194/bgd-6-5163-2009.

Smith, M.E., Carroll, A.R., and Singer, B.S., 2008, Synoptic reconstruction of a major ancient lake system: Eocene Green River Formation, western United States: Geological Society of America Bulletin, v. 120, no. 1, p. 54–84, doi: 10.1130/B26073.1.

Sommerfield, C.K., and Nittrouer, C.A., 1999, Modern accumulation rates and a sediment budget for the Eel shelf: A flood-dominated depositional environment: Marine Geology, v. 154, no. 1–4, p. 227–241, doi: 10.1016/S0025-3227(98)00115-7.

Straub, K.M., and Wang, Y., 2013, Influence of water and sediment supply on the long-term evolution of alluvial fans and deltas: Statistical characterization of basin-filling sedimentation patterns: Journal of Geophysical Research: Earth Surface, v. 118, p. 1602–1616, doi: 10.1002/jgrf.20095.

Teague, W.J., Jarosz, E., Keen, T.R., Wang, D.W., and Hulbert, M.S., 2006, Bottom scour observed under Hurricane Ivan: Geophysical Research Letters, v. 33, no. 7, p. 1–3, doi: 10.1029/2005GL025281.

Tooth, S., 2005, Splay Formation Along the Lower Reaches of Ephemeral Rivers on the Northern Plains of Arid Central Australia: Journal of Sedimentary Research, v. 75, no. 4, p. 636–649, doi: 10.2110/jsr.2005.052.

Torricelli, S., Knezaurek, G., and Biffi, U., 2006, Sequence biostratigraphy and paleoenvironmental reconstruction in the Early Eocene Figols Group of the Tremp-Graus Basin (south-central Pyrenees, Spain): Palaeogeography, Palaeoclimatology, Palaeoecology, v. 232, no. 1, p. 1–35, doi: 10.1016/j.palaeo.2005.08.009.

Ulrich, J., 2016, TTR: Technical Trading Rules:

Vandenberghe, N., Hilgen, F.J., Speijer, R.P., Ogg, J.G., Gradstein, F.M., Hammer, O., Hollis, C.J., and Hooker, J.J., 2012, The Paleogene Period, *in* Gradstein, F.M., Ogg, J.G., Schmitz, M.D., and Ogg, G. eds., The Geologic Time Scale, Elsevier B. V., Boston, p. 855–921.

Walsh, J.P., Corbett, D.R., Kiker, J.M., Orpin, A.R., Hale, R.P., and Ogston, A.S., 2014, Spatial and temporal variability in sediment deposition and seabed character on the Waipaoa River margin, New Zealand: Continental Shelf Research, v. 86, p. 85–102, doi: 10.1016/j.csr.2014.07.001.

Wiberg, P., 2000, A Perfect Storm: Formation and Potential for Preservation of Storm Beds on the Continental Shelf: Oceanography, v. 13, no. 3, p. 93–99, doi: 10.5670/oceanog.2000.18.

Yee, T.W., 2015, Vector Generalized Linear and Additive Models: With an Implementation in R: